Cascade excitation of vortex motion and reentrant superconductivity in flexible Nb thin films

Liping Zhang(张丽萍)[1,2,†], Zuyu Xu(徐祖雨)[3], Xiaojie Li(黎晓杰)[3], Xu Zhang(张旭)[2], Mingyang Qin(秦明阳)[2,4], Ruozhou Zhang(张若舟)[2,5], Juan Xu(徐娟)[2], Wenxin Cheng(程文欣)[2,5], Jie Yuan(袁洁)[2,6], Huabing Wang(王华兵)[3,7], Alejandro V. Silhanek[8], Beiyi Zhu(朱北沂)[2], Jun Miao(苗君)[1], and Kui Jin(金魁)[2,5,9]

[1] *School of Materials Science and Engineering, University of Science and Technology Beijing, Beijing* 100083, *China*
[2] *Beijing National Laboratory for Condensed Matter Physics, Institute of Physics, Chinese Academy of Sciences, Beijing* 100190, *China*
[3] *Research Institute of Superconductor Electronics, School of Electronic Science and Engineering, Nanjing University, Nanjing* 210023, *China*
[4] *Department of Materials Science and Engineering, Southern University of Science and Technology, Shenzhen* 518055, *China*
[5] *School of Physical Sciences, University of Chinese Academy of Sciences, Beijing* 100049, *China*
[6] *Key Laboratory of Vacuum Physics, School of Physical Sciences, University of Chinese Academy of Sciences, Beijing* 101408, *China*
[7] *Purple Mountain Laboratories, Nanjing* 211111, *China*
[8] *Experimental Physics of Nanostructured Materials, Q-MAT, CESAM, Université de Liège, B*-4000 *Sart Tilman, Belgium*
[9] *Songshan Lake Materials Laboratory, Dongguan* 523808, *China*

(Received 21 October 2022; revised manuscript received 2 December 2022; accepted manuscript online 16 December 2022)

High quality Nb films were successfully prepared on both flexible polyimide (PI) and rigid Al_2O_3 substrates and their transport properties were systematically studied at various applied currents, external magnetic fields, and sample orientations. It is found that a curved Nb/PI film exhibits quite different superconducting transition and vortex dynamics compared to the flat Nb/Al_2O_3 film. For the curved Nb/PI film, smooth superconducting transitions were obtained at low currents, while unexpected cascade structures were revealed in the $\rho(T)$ curves at high currents. We attribute this phenomenon to the gradient distribution of vortex density together with a variation of superconductivity along the curved film. In addition, reentrant superconductivity was induced in the curved Nb/PI thin film by properly choosing the measurement conditions. We attribute this effect to the vortex pinning from both in-plane vortices and out-of-plane vortices. This work reveals the complex transport properties of curved superconducting thin films, providing important insights for further theoretical investigations and practical developments of flexible superconductors.

Keywords: vortex dynamics, flexible superconducting films, transport properties, superconducting films

PACS: 73.61.–r, 74.25.Wx, 74.78.–w **DOI:** 10.1088/1674-1056/acac16

1. Introduction

It is well known that, in type-II superconductors, the magnetic field penetrates in the form of quantized vortices when lying between the lower (H_{c1}) and upper (H_{c2}) critical magnetic fields.[1] In the past few decades, a great deal of attention has been paid to the investigation of vortex matter in superconductors due to their rich interesting phenomena and complex dynamical vortex phase diagrams,[2,3] arising from the interplay among vortex pinning, vortex–vortex interaction, and thermal fluctuations. Additionally, understanding vortex dynamics is fundamental for the development of technological applications of superconducting materials. On the one hand, the vortex motion always causes unwanted dissipation in superconducting wires and superconducting radio-frequency cavities.[4–6] On the other hand, controlling the vortex motion is essential for many novel devices such as vortex rectifiers,[7–9] superconducting quantum interference devices,[10] single photon detectors,[11,12] and flux qubits.[13,14]

Thus far, most of fundamental and practical researches related to vortex matter have been carried out on superconducting thin films grown on rigid substrates, whereas flexible superconducting thin films[15–18] seem to slowly catch up with the new trend on frontier sciences and technologies. Many flexible electronic materials and exciting products have been discovered and manufactured,[19] such as E-skin in robotics and prosthetics,[20] biomedical instruments,[21] flexible batteries,[22] flexible electrodes[23] and flexible display devices.[24] Although the vortex properties in bulk superconductors with curvilinear surface, such as cylinders[25] or balls,[26,27] have been preliminarily studied in theory, detailed experimental measurements on the vortex dynamics in flexible superconducting films are still in their infancy.[28]

In this paper, we have successfully prepared high quality Nb films on both flexible polyimide (PI) and rigid Al_2O_3 substrates, respectively. By detailed measurements of transport properties in the two systems, we have found that the vortex dynamics in curved superconducting films is different from that in the flat ones. Unexpected discontinuous jumps or cascade structures appear in the $\rho(T)$ curves of the curved Nb/PI

†Corresponding author. E-mail: lipingzhang@iphy.ac.cn
© 2023 Chinese Physical Society and IOP Publishing Ltd

film at relatively high applied currents, which can be attributed to the gradient distribution of vortex density and the variation of superconductivity in the curved structures under an external magnetic field. Additionally, a reentrant superconducting phase has also been revealed in the curved Nb/PI film for certain orientations of the applied field and applied currents. This work provides new insight on the physics of flexible superconducting materials and hopefully stimulates the theoretical studies paving the way to future technological applications.

2. Experiments

The chosen PI substrate has tremendous potential in various practical applications[29] because of its excellent optical transparency, electric insulation, and marvellous bendable properties. Most importantly, the wide and stable service temperature range of -200 °C to 300 °C enables it to be one of the best substrate candidates for the study of flexible superconducting electronics. Here, we employed the magnetron sputtering technique to fabricate Nb films on both flexible PI and rigid Al_2O_3 substrates with thickness $d \approx 100$ nm.[30,31] The surface of the Nb/PI film was quite smooth as seen in Fig. A1 of Appendix A. Subsequently, we patterned a six-terminal bridge by photolithography and ion beam etching, where the width $w = 40$ μm and the length $l = 800$ μm, as shown in the inset of Fig. 2(b). To study the transport properties and vortex matter of the superconducting thin film, we fabricated an aluminium alloy block with curved surface permitting to bend the flexible superconducting film, and the block was mounted onto the puck which could be rotated by the rotating rod. The resistivity was measured by a Keithley 6221 current source and a Keithley 2182 nanovoltmeter at low temperature and magnetic field environments provided by the physical property measurement system (PPMS).

3. Results and discussion

3.1. Basic properties of flat Nb/PI and Nb/Al_2O_3 films

We measured the temperature dependence of the resistivity $\rho(T)$ curves of flat Nb/PI and Nb/Al_2O_3 films at different magnetic fields. As shown in Fig. 1, for $H = 0$ T the zero-resistance critical superconducting transition temperatures (T_{c0}) of both Nb/PI and Nb/Al_2O_3 samples are 8.7 K and 9.0 K, respectively. With the increase of the magnetic field, the superconducting transitions remain sharp, which indicates high quality samples. In addition, when the magnetic field is about ~ 1 T, T_{c0} of Nb/PI is clearly larger than that of Nb/Al_2O_3, which suggests that the Nb/PI has a stronger vortex pinning effect likely from the rough surface of the PI substrates.[32] In order to compare the superconducting properties of both curved and flat Nb films more precisely, the subsequent measurements were mainly carried out at a magnetic field $H = 0.5$ T, where both films with different substrates have quite similar T_{c0} values, as shown in Figs. 1(a) and 1(b).

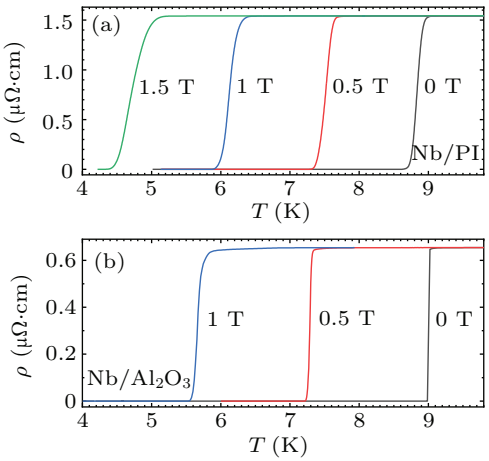


Fig. 1. Resistivity versus temperature curves at various magnetic fields for (a) pristine flat Nb/PI film and (b) Nb/Al_2O_3 film, with the applied current $I = 50$ μA for all the measurements.

3.2. The $\rho(T)$ at low currents

In order to study the vortex dynamics of flexible superconductors, we measured the electrical transport properties of the curved Nb/PI film for different orientations at a fixed magnetic field and low applied current $I = 50$ μA, corresponding to a current density $J = \frac{I}{w \times d} = 1.25 \times 10^3$ A/cm^2. The schematic of rotation measurement setup is shown in the inset of Fig. 2(a). The angle θ is defined between the direction of the magnetic field and the normal to the film surface. For the curved Nb/PI film, the central angle of the curved bridge is 10° and the corresponding radius $r \approx 4.58$ mm, as seen in the inset of Fig. 2(a). The strain caused by the curved substrate on the Nb film can be estimated as $\epsilon = d/(2r+d) \approx 1 \times 10^{-5}$, which is negligible due to the small value.[54] Besides, since the bending model remains unchanged during our experiments, the strain is always the same for different measurement angles, and then the influence caused by the strain is constant. Therefore, it is reasonable to neglect the strain effect in the present study. Therefore, we would like to emphasize that our exploration only focuses on the vortex motion induced by the geometric deformation of the sample after bending.

In Fig. 2, we show the $\rho(T)$ curves of both cool-down and warm-up measurements for the curved Nb/PI film and flat Nb/Al_2O_3 film with different θ values at $I = 50$ μA. With increasing θ, T_c^{onset} increases and the superconducting transition temperature width between T_c^{onset} and T_{c0} becomes wider. Here, T_c^{onset} is the onset temperature of the superconducting transition from the normal state to the mixed state, where superconducting condensation begins to occur.

Let us now clarify whether the evolution of T_c^{onset} versus θ is determined by the decrease of the normal component of the magnetic field $H_\perp$. We plot T_c^{onset} as a function of the feature perpendicular components $H_\perp = H\cos\theta$ in such a way

to build $H_{c2}(T)$ for the Nb thin film. From Ginzburg–Landau expression $H_{c2}(T) = \frac{\Phi_0}{2\pi\xi^2(T)}$, with $\Phi \approx 2.07 \times 10^{-15}$ Wb, we infer $\xi(0) = \left[-\frac{\Phi_0}{2\pi T_c}\frac{dT}{dH_{c2}(T)}\right]^{\frac{1}{2}}$. Taking into account $T_c^{onset} \approx 8.3$ K and $dT/dH_{c2} \approx -2.13$ [K/T] estimated from Fig. 2(b), we can roughly obtain a very reasonable coherence length of $\xi_0 \approx 9.2$ nm for the Nb thin film, which is quite similar to the previous studies.[33,34] This seems to suggest that T_c^{onset} increases since the normal component of the magnetic field $H_\perp$ decreases.

In addition, the $\rho(T)$ curves exhibit an unexpected kink at T^* for both curved and flat cases at relatively large θ. One can clearly see that the $\rho(T)$ kink of curved Nb/PI film is smoother than that of flat Nb/Al_2O_3 film at the same θ. With the decrease of θ, the kink features gradually disappear at 45° for the curved Nb/PI film and 15° for the flat Nb/Al_2O_3 film as indicated by the dashed lines in Figs. 2(a) and 2(b). In fact, irrespective of whether the sample is curved or flat, the $\rho(T)$ behaviors are quite similar at low current. We speculate that with the increase of temperature, there exist two different superconducting transitions in the $\rho(T)$ curves at larger θ values, where the external magnetic field exhibits an important component parallel to the film.

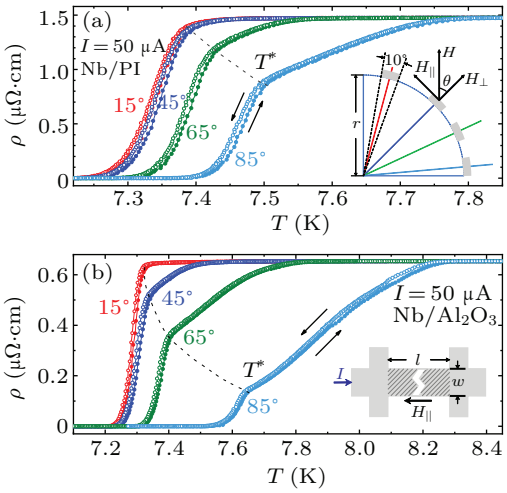


Fig. 2. The hollow circle and solid circle lines represent the data from cool-down and warm-up $\rho(T)$ measurements, for both (a) the curved Nb/PI film and (b) the flat Nb/Al_2O_3 film with $\theta = 15°$, 45°, 65° and 85° at $H = 0.5$ T and $I = 50$ μA ($J = 1.25 \times 10^3$ A/cm^2). The pair of opposite arrows indicate the temperature sweeping direction. T^* and the dashed line indicate the temperature where the kink occurs and its dependence on the angle θ. The inset in (a) displays the orientation θ for both curved and flat films in the vertical magnetic field, where θ expresses the angle between the direction of magnetic field and the normal to the film surface. Additionally, $H_\perp$ and $H_\parallel$ represent the components of the magnetic field perpendicular and parallel to the surface of the film, respectively. The inset in (b) shows the six-terminal bridge for both the curved and the flat films in our measurements, where the width w and length l of the bridge are 40 μm and 800 μm, respectively.

3.3. The $\rho(T)$ at high currents

In this section, we will investigate the effect of the applied current on the vortex dynamics for both the curved Nb/PI and the flat Nb/Al_2O_3 films by measuring the $\rho(T)$ curves at different film orientations in the external magnetic field with 1 mA and 10 mA, respectively. As shown in Fig. 3, the transition temperatures T_{c0} for both films are clearly reduced as compared with the similar measurements at low current in Fig. 2, because the high current not only depletes the superconducting condensate but also provides enough force to drive the pinned vortices and set them in motion at relatively low temperatures.

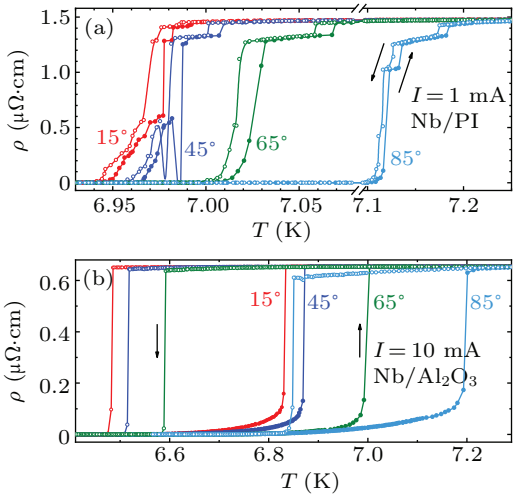


Fig. 3. The temperature dependence of the hysteretic resistivity $\rho(T)$ for (a) curved Nb/PI film with $I = 1$ mA ($J = 2.5 \times 10^4$ A/cm^2), and (b) flat Nb/Al_2O_3 film with $I = 10$ mA ($J = 2.5 \times 10^5$ A/cm^2), measured at $H = 0.5$ T and $\theta = 15°$, 45°, 65° and 85°.

In the case of high applied currents, the $\rho(T)$ curves of the curved Nb/PI film are clearly different from those of the Nb/Al_2O_3 film. For the curved Nb/PI film, an unexpected cascade structure in the $\rho(T)$ curve develops for almost all the film orientations with respect to the external magnetic field. In other words, the resistivity of the curved Nb/PI film undergoes a sequence of plateau structures by decreasing or increasing temperatures. To our knowledge, this behavior of $\rho(T)$ dependence has not been reported so far. In fact, we have systematically measured the $\rho(T)$ response for a series of θ values by rotating both the curved Nb/PI and the flat Nb/Al_2O_3 films in a fixed magnetic field. As shown in Fig. 3(a), for almost all the film orientations there exists a prominent plateau structure in the $\rho(T)$ curves around ~ 1.3 μΩ·cm corresponding to the fast vortex motion. With increasing θ, the temperature window of this plateau becomes wider. When the film bridge is almost parallel to the magnetic field at large θ values, intermediate plateaus appear and the corresponding resistance value is around ~ 1.1 μΩ·cm.

The behavior of geometrically anisotropic superconductors in magnetic fields, especially the vortex crossing or the interaction between perpendicular and longitudinal magnetic fields in superconducting thin films, is a long-standing research topic.[37] Although the vortex cutting-reconnection phenomenon is not yet clearly understood, numerous experiments have demonstrated that the vortex crossing has

a considerable effect on the vortex dynamics. Interestingly, when the Nb/PI film is close to $\theta = 45^\circ$ as shown in Fig. 3(a), the reentrant superconductivity phenomenon occurs, i.e., non-zero resistances below T_{c0} appear again at low temperatures, which has been reported in a large variety of superconductors.[44–50,55]

We have found that the reentrant superconductivity can be obtained in the curved sample at small θ and low currents or at large θ and high currents, as shown in Figs. 3(a) and 6(a). The reentrant superconductivity is a nontrivial phenomenon, which combines many factors including pinning, applied current intensity, sample size, etc. For example, in our experiments, the reentrant superconductivity as well as the $\rho(T)$ step structure cannot be measured at low applied current even in the curved Nb/PI film, as shown in Fig. 2(a). Nevertheless, in the transport measurement of the micro-narrow superconducting system, with the increase of the magnetic field, the alternating appearance of periodic and random vortex line lattices can also lead to the emergence of reentrant superconductivity and even magnetoresistive oscillation due to the strong boundary pinning effect.[51]

For the flat Nb/Al_2O_3 film, both the resistivity cascade feature and the reentrant superconductivity phenomena are absent in the $\rho(T)$ curves, even if the applied current increases up to 10 mA, as shown in Fig. 3(b). Additionally, the $\rho(T)$ curves of the Nb/Al_2O_3 film exhibit very large hysteresis behavior at high applied currents due to heating caused by the fast-moving vortices during the cool-down process.

3.4. Gradient distribution of vortex density in the curved superconducting film

In this section, we propose a simple vortex lattice model based on previous experimental and theoretical works[38–40] to explain the vortex distribution in the curved film. Since Nb is an s-wave superconductor, the vortex lattice is supposed to be triangular at high enough magnetic fields.[41] When $\theta = 0^\circ$, i.e., the magnetic field is perpendicular to the film, the hexagon is circumscribed by a circle with radius a satisfying $a^2 = 2\Phi_0/\sqrt{3}H$, where Φ_0 is the vortex quantum, as shown in the upper panel of Fig. 4(a). When $\theta > 0^\circ$, the high symmetry of the vortex lattice will be broken, and as a result the isotropic circle will be stretched into an ellipse with the major semiaxis of $a/\cos\theta$, as shown in the lower panel of Fig. 4(a). In this case, the number of vortices in the flat Nb/Al_2O_3 film, n, satisfies $n\Phi_0 = H \cdot S$, where $S = wl\cos\theta$ is the projected area of the bridge in the horizontal plane. For the curved Nb/PI film, we use the chord of the curved bridge $l' = 2r \cdot \sin\left(\frac{l}{r} \cdot \frac{180^\circ}{\pi}\right) \approx 799$ μm to calculate the effective area, as shown in the insets of Fig. 4(b). Then, we calculate the real vortex number n in the bridge for both curved Nb/PI and flat Nb/Al_2O_3 films at various orientations in the magnetic field, and the number n decreases with increasing θ and drops rapidly near 90°, as shown in Fig. 4(b).

In order to understand the change in the number of vortices in the bridge area depending on the sample orientation, we draw the schematics of vortex lattice structure within 0.5×0.5 μm^2 at different values of θ, as shown in Figs. 4(c)–4(e). For example, at $\theta = 0^\circ$, the vortex number n satisfies $n\Phi_0 = H \cdot S = 0.5T \times 0.5$ μm$\times 0.5$ μm$\approx 60\Phi_0$ in the designated area. In an ideal scenario, if the vortex tube inside the film is perfectly aligned along the direction of the applied magnetic field, the expected shape of each vortex at the film surface would be close to an ellipse with the minor semiaxis of ξ and the major one of $\sim \xi/\cos\theta$, where ξ is the coherence length of superconductors. However, when θ is large, the major is much longer than the minor as shown in Figs. 4(c)–4(e) by the orange insets. This exaggerated ellipse is inconsistent with previous experimental observations,[35,39,40,42,43] which confirmed that vortex tubes tend to be perpendicular to the film surface and the shape of each vortex at the surface will not be much deformed. Therefore, we have modified the size and shape of the individual vortex according to the previous experimental works.[38–40]

Next, we provide a schematic diagram of the vortex distribution in a quadrant circular curved system in Fig. 5 to explain the $\rho(T)$ cascade structures measured under an applied magnetic field. The vortex density in the curved film is distributed with a certain gradient as shown in Fig. 5, where we also indicate the tangential and normal components of the magnetic field at different angles on the sample surface. With the increase of the sample orientation angle θ, the normal component of the magnetic field $H_\perp$ gradually decreases from H to 0, while the tangential component of the magnetic field $H_\parallel$ gradually increases from 0 to H.

In fact, in the uniform magnetic field shown in Fig. 5, the bending of the superconducting film causes not only the gradual decrease of the vortex density with the increase of θ in the sample but also a continuous change of the superconducting critical transition temperature T_c, critical magnetic field H_c and critical current J_c along the bending direction. Early classic theories and experiments have confirmed that the nucleation of superconductivity in decreasing fields should always first occur near the material surface.[52,53] More importantly, it has been revealed that the layer material or thin film can remain superconducting in magnetic fields larger than the maximum bulk critical field H_c or H_{c2} for type-I or II superconductors, respectively. When the magnetic field is parallel to the superconductor surface, the system withholds higher magnetic fields up to the third upper critical field for the surface nucleation of superconductivity given by $H_{c3} = 1.69H_{c2}$.[52,53]

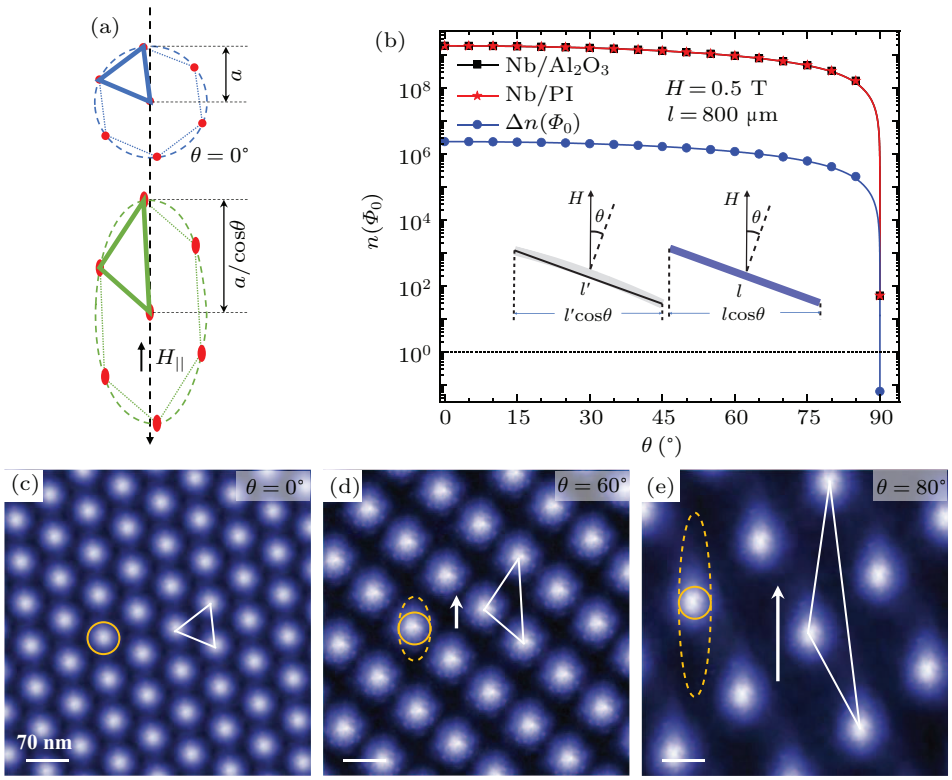


Fig. 4. (a) Schematics of the vortex lattice features at $\theta = 0°$ (upper panel), i.e., the magnetic field is perpendicular to the superconducting film surface, and the case of $\theta \neq 0°$ (lower panel) assuming that vortices do not bend at the sample surface. The red solid dots represent the locations of the individual quantum vortices. (b) Number of vortices versus θ for both flat Nb/Al_2O_3 (black square line) and curved Nb/PI (red star line) films in the whole bridge area of 800 μm×40 μm shown in Fig. 2(b) inset. The blue line with scattered solid circles gives the number difference of vortices between flat Nb/Al_2O_3 and curved Nb/PI bridge areas by the black square line value subtracting the red star line value. The insets illustrate the projection of the bridge length l for the Nb/Al_2O_3 film and the chord of the curved bridge l' for the Nb/PI film in the horizontal plane at certain orientation θ in the vertical magnetic field. (c)–(e) Illustrations of the vortex lattice structures in a square area of 0.5 μm×0.5 μm with different film orientations $\theta = 0°$, 60° and 80°. The rotation axis is horizontal and the white arrows indicate the stretching direction of the vortex lattices. The radius of the orange solid line circle is $\sim \xi$, and the major semiaxis of the orange dotted line ellipse is $\sim \xi/\cos\theta$. The orange circle and ellipse represent the quantum vortices in the film which are perpendicular or tilted to the magnetic field in ideal scenarios, respectively.

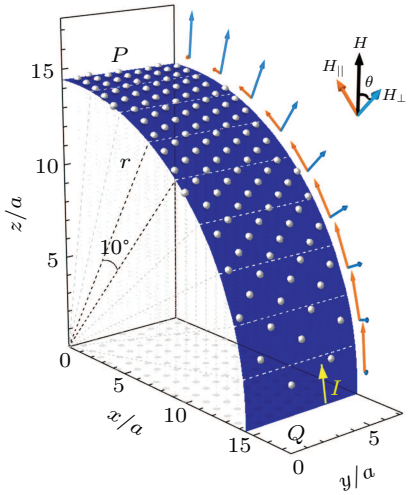


Fig. 5. Illustration of the vortex density distribution in a quadrant circularly curved superconducting film from P to Q with radius r in the vertical and uniform magnetic field H. The orange and blue arrows indicate the $H_{||}$ and $H_\perp$ components, respectively, which are varied with θ. The dashed lines indicate the variation of the similar measurement positions with θ. Here, the width of the curved sample is $y = 0.5$ μm and the length of the arc surface is $\pi r/2$ with the radius $r = 1$ μm. The applied magnetic field is $H = 0.5$ T, and the yellow arrow indicates the applied current. The scale unit of the coordinate axis is the lattice constant $a \approx 69$ nm of the projected equilateral triangles on the horizontal plane. P and Q indicate that the sample orientation is at $\theta = 0°$ and $\theta = 90°$, respectively.

Therefore, thin films with various orientations to the magnetic field should have different upper critical fields, which can be defined as $H_{c2}(\theta)$. In the curved superconducting sample shown in Fig. 5, the sample side P represents that the applied magnetic field is perpendicular to the sample surface $H_\perp = H$, and its upper critical field is $H_{c2}^Q = H_{c2}(\theta = 0°) = H_{c2}$. As the angle θ increases, the magnetic field $H_{||}$ parallel to the film gradually dominates. At side Q as seen in Fig. 5, H is completely parallel to the film plane, where the upper critical field should be the surface superconducting critical field, i.e., $H_{c2}^Q = H_{c2}(\theta = 90°) = H_{c3} > H_{c2}^P$.

The existence of vortex matter in the mixed state is mainly restricted by the upper critical field of the superconductor. When the sample orientation θ is small, the perpendicular component of the magnetic field $H_\perp = H\cos\theta$ plays a more relevant role than $H_{||}$. In contrast, when the sample orientation angle θ is large enough, the parallel component $H_{||}$ dominates. We propose that the $\rho(T)$ step jumps are mainly ruled by the proximity to the upper critical field H_{c2} of the curved samples at different orientations. From another point of view, according to Brandt and Valsko-Vlasov,[36,37] the vortices perpendicular to $H_{||}$ are difficult to move. Therefore, for a fixed H, the

larger the θ, the larger the $H_{\parallel}$. As θ increases, this effect also tends to increase J_c.

We have shown $\rho(T)$ curves for various orientations of the curved Nb/PI thin film at $H = 0.5$ T in Fig. 2(a), and one can clearly see the dependence of the critical transition temperatures of both T_{c0} and T_c^{onset} on the film orientation θ. In an external magnetic field, T_{c0} in the small θ area of the curved film is relatively low due to suppression by the high normal field component $H_{\perp}$, as seen in Fig. 5. Therefore, driven by an applied current, the vortices in the small θ area are easy to depin and move, resulting in a finite electrical resistivity, while the vortices in other parts of the sample remain pinned. With the increase of temperature, the velocity of the vortices will increase due to the stronger vortex–vortex interaction and weakened pinning effect in the vortex flow region, which will lead to a small tilt in each $\rho(T)$ step, as seen in Fig. 3(a). When the temperature is high enough, the vortices in the large θ regions can also be depinned step by step and join the contribution of the resistivities by the applied current, which leads to jumps in the $\rho(T)$ curves, as seen in Fig. 3(a).

We conclude that for a curved superconducting thin film in a permanent magnetic field, the vortex motion at different sample regions is quite different. While in the flat system, all the vortex dynamic processes in the whole sample should be always the same for any condition of temperature and sample orientation. This scenario can account for the absence of step features in the $\rho(T)$ curves of the flat Nb/Al_2O_3 film in Fig. 3(b). Therefore, we attribute the cascade structure in the $\rho(T)$ curve to the gradient distribution of vortex density and the continuous variation of superconductivity with the orientation θ of the curved film, which leads to the different mobility of vortex bundles along the curved direction in the sample. In other words, the cascade structure of $\rho(T)$ might be due to the step depinning of vortex lattices in plastic motion and coexisting of pinned and mobile vortices in the curved sample.

4. Dependence of $\rho(T)$ cascade structure on the applied current magnetic field

According to the experimental measurements in Figs. 2 and 3 and the phenomenological theory analyses above, the appearance of the cascade structures in the $\rho(T)$ curves of the curved Nb/PI film is not only dependent on its orientation in the magnetic field but also significantly influenced by the external current. Thus, we have systematically measured the $\rho(T)$ curves of both the curved Nb/PI and the flat Nb/Al_2O_3 films for various currents at constant $\theta = 65°$ and $H = 0.5$ T. The superconducting transition for both curved Nb/PI and flat Nb/Al_2O_3 films becomes sharp with the increase of the applied currents due to the strong heating effects, as shown in Figs. 6(a) and 6(b).

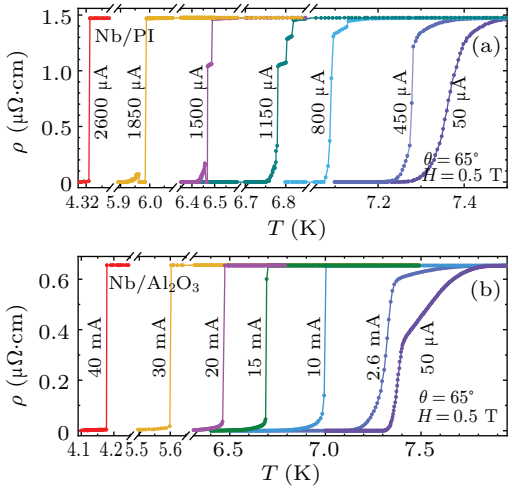


Fig. 6. The $\rho(T)$ curves measured at $\theta = 65°$ and $H = 0.5$ T at various applied currents, for (a) the curved Nb/PI film, $I = 50$ μA, 450 μA, 800 μA, 1150 μA, 1500 μA, 1850 μA and 2600 μA, and the corresponding current densities $J = 1.25 \times 10^3$ A/cm^2, 1.125×10^4 A/cm^2, 2.0×10^4 A/cm^2, 2.875×10^4 A/cm^2, 3.75×10^4 A/cm^2, 4.625×10^4 A/cm^2, and 6.5×10^4 A/cm^2, (b) the flat Nb/Al_2O_3 film, $I = 50$ μA, 2.6 mA, 10 mA, 15 mA, 20 mA, 30 mA and 40 mA, and the corresponding current densities $J = 1.25 \times 10^3$ A/cm^2, 6.5×10^4 A/cm^2, 2.5×10^5 A/cm^2, 3.75×10^5 A/cm^2, 5.0×10^5 A/cm^2, 7.5×10^5 A/cm^2, 1.0×10^6 A/cm^2, respectively.

In Fig. 6(a), the cascade structure does not appear until the applied current increases up to ~ 800 μA. In the case of 1150 μA, there exist two clear resistivity plateaus in the $\rho(T)$ curve around ~ 1.3 μΩ·cm and ~ 1.1 μΩ·cm. When the current increases to 1500 μA, the resistivity plateau at ~ 1.3 μΩ·cm disappears and the signal of reentrant superconductivity develops with decreasing temperature. Further increasing the applied current, both the cascade structure and the reentrant superconductivity phenomenon in the $\rho(T)$ curves of the Nb/PI film gradually disappear, because the temperature width between T_c^{onset} and T_{c0} for the superconducting transition is highly suppressed, as shown in Fig. 6(a) at extremely high applied currents.

Based on the analyses in Subsection 3.4, the existence of the cascade structure in the $\rho(T)$ curves of the curved Nb/PI film is also dependent on the vortex–vortex interaction, which is determined by the temperature dependent penetration depth λ. The vortex–vortex interaction weakens severely if the temperature is far below the thermodynamical superconducting transition temperature $T_c \approx 8.7$ K.

The negligible vortex–vortex interaction in very low temperatures can also help us to understand why the cascade structure as well as the reentrant superconductivity in the curved Nb/PI film fades away at high applied currents. In addition, for the flat Nb/Al_2O_3 film in Fig. 6(b), there is no signal of the cascade structure and reentrant superconductivity in the $\rho(T)$ curves, even if the applied current is increased up to 40 mA.

In Fig. 7, we show the dependence of $\rho(T)$ cascade structures in the curved Nb/PI film on the magnetic field at constant $\theta = 65°$ and $I = 1$ mA. The $\rho(T)$ curves always exhibit sharp superconducting transitions for various magnetic fields.

With the increase of the magnetic field, the resistivity plateau at $\sim$ 1.3 μΩ·cm shrinks and gradually disappears at about 1.1 T. Besides, another resistivity plateau around $\sim$ 0.5 μΩ·cm emerges at 0.7 T, and the corresponding temperature region expands with the increase of the magnetic field till 1.4 T. The two resistivity plateaus coexist between $\sim$ 5.1 K and $\sim$ 6.4 K when $H \approx 0.7$ T–1.1 T. Notice that there is no reentrant superconductivity phenomenon for any of the magnetic field applied, because the film orientation θ is too large or the current is not high enough as discussed in Figs. 3(a) and 6(a).

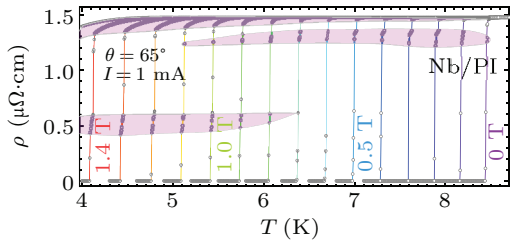


Fig. 7. The $\rho(T)$ curves of the curved Nb/PI film measured at constant $\theta = 65°$ and $I = 1$ mA ($J = 1.25 \times 10^3$ A/cm^2) for a series of magnetic fields from 0 T to 1.5 T with an interval of 0.1 T. The pink regions show the evolution of the individual $\rho(T)$ steps with the magnetic fields.

5. Conclusion and perspectives

In summary, we have successfully grown high quality Nb films on both flexible PI and rigid Al_2O_3 substrates and systematically investigated the transport properties of the films under magnetic field, electric current and for several sample orientations. When the applied current is weak, a smooth superconducting transition is observed for both samples. However, when the applied current is high enough, a series of resistivity drops appear in the curved Nb/PI films, with no counterpart in the flat Nb/Al_2O_3 film. We find that the $\rho(T)$ step structures depend on the film orientation, the applied current and the magnetic field. We attribute the step structures in the $\rho(T)$ curve to the gradient distribution of vortex mobility and the variation of superconductivity with the orientation θ of the curved sample in the external magnetic field. Additionally, we have also obtained the reentrant superconductivity phenomenon in the transport measurements of the curved Nb/PI film for a certain combination of applied currents, magnetic fields, and film orientations.

We believe that these transport measurements together with the analysis of the vortex dynamics in curved superconducting films unveil a rich diversity of phenomena with no counterpart in flat films. Above all, the flexible superconductor is a crucial frontier topic in superconductivity research, and possesses great potential for magnetic field sensing, bolometry, and fluxonic devices. This work provides a new platform for investigating flexible superconductors and facilitating rapid transitions from laboratory demonstrations to industrial prototypes and actual products.

Appendix A: Surface morphologies of Nb/PI films

Morphological changes are unavoidable for Nb/PI samples due to their flexible properties. In order to explore whether the deformation will damage the surface of the Nb/PI film, we used a Hitachi SU5000 field-emission scanning electron micrograph (SEM) to detect the microstructures of the sample. The film surfaces of different magnifications are shown in Fig. A1. It is clearly that the surface topography is uniform on a macro scale, and it has less grain impurities on the surface in Fig. A1(a). In the case of high resolution, we can see that the surface in Fig. A1(b) is also very smooth. More importantly, the surface of the film is compact and free of microcracks and micropores. Anyway, the SEM micrographs confirm the high quality of our Nb/PI samples.

Subsequently, we investigate the surface morphology of the flexible Nb/PI film on the curved holder with a microscope (SKU:NI-Eclipse-LV150N). The whole curved bridge of the Nb/PI film is captured in Fig. A2(a), and some middle areas are zoomed in as shown in Figs. A2(a)–A2(c). All the images in Fig. A2 reveal a homogenous and relatively smooth surface, even though there exist a few isolated granular defects, which may be affected by the intrinsic defects of the polymer substrate PI or arise from the sample preparation process.[56]

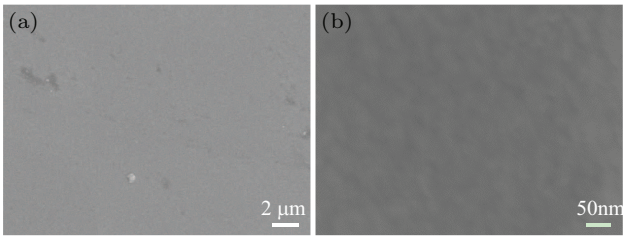


Fig. A1. SEM images of the flat Nb/PI film for both (a) low and (b) high resolution.

Above all, we want to emphasize that these images of the sample surface in Fig. A2 were taken directly on the sample stage after low temperature measurement, which confirm that the low temperature environment does not have a significant effect on the surface of Nb/PI and there is not any crack. These investigations suggest that the Nb/PI films have excellent characteristics of flexibility and mechanical properties. Since the substrate PI is an organic flexible material, not a single crystal, the adhesion of the superconducting niobium film on the PI surface is very weak. In addition, the metal niobium film has a certain degree of flexibility and ductility. In the case of a small bending curvature of the sample, the superconducting niobium film deforms very little and does not produce destructive defects such as cracks. The stress in the niobium film has no significant influence on the vortex dynamics explored in the present work.

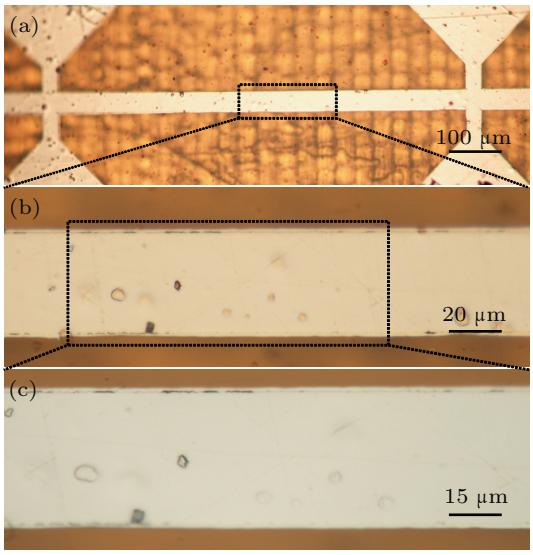


Fig. A2. Photos of the real Nb/PI bending film on the curved holder used in the present work for different magnifications (a)–(c).

Appendix B: Time dependence of temperature and resistivity

In Fig. B1, we plot the time dependence $\rho(t)$ and $T(t)$ curves of a bending sample at $\theta = 45°$ measured in Fig. 3(a), which shows both reentrant superconductivity and resistivity plateau phenomena on the $\rho(T)$ curve. The temperature does not change abruptly at the time when the reentrant superconductivity and plateau phenomenon appear as shown in Fig. B1. Therefore, the influence of overheating effect on resistivity behaviors of our measurements in the superconducting samples could be neglectable.

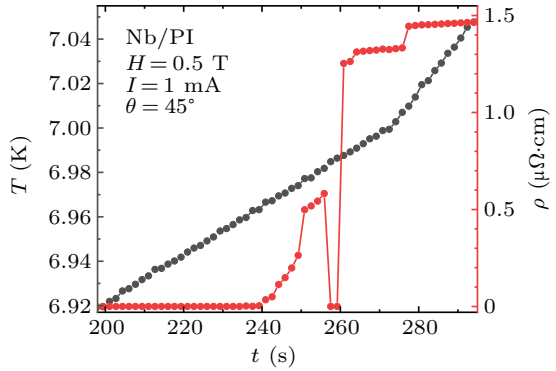


Fig. B1. The time dependence $\rho(t)$ and $T(t)$ curves of curved Nb/PI film measured at $\theta = 45°$, $H = 0.5$ T and $I = 1$ mA and the corresponding current density $J = 2.5 \times 10^3$ A/cm^2.

Acknowledgements

Project supported by the National Key Basic Research Program of China (Grant Nos. 2021YFA0718700, 2018YFB0704102, 2017YFA0303003, 2017YFA0302902, 2016YFA0300301, and 2021YFA0718802), the National Natural Science Foundation of China (Grant Nos. 11927808, 11834016, 118115301, 119611410, 11961141008, 61727805, and 11961141002), the Key Research Program of Frontier Sciences, Chinese Academy of Sciences (CAS) (Grant Nos. QYZDB-SSW-SLH008 and QYZDY-SSW-SLH001), CAS Interdisciplinary Innovation Team, the Strategic Priority Research Program (B) of CAS (Grant Nos. XDB25000000 and XDB33000000), the Beijing Natural Science Foundation (Grant No. Z190008), and the Key-Area Research and Development Program of Guangdong Province, China (Grant No. 2020B0101340002). M.Q. thanks the support from the China Postdoctoral Science Foundation (Grant No. 2022M711497).

References

[1] Tinkham M 1996 *Introduction to superconductivity* (New York: McGraw-Hill)
[2] Blatter G, Feigel'man M V, Geshkenbein V B, Larkin A I and Vinokur V M 1994 *Rev. Mod. Phys.* **66** 1125
[3] Zhu B Y, Marchesoni F, Moshchalkov V V and Nori F 2003 *Phys. Rev. B* **68** 014514
[4] Pathirana W P M R and Gurevich A 2021 *Phys. Rev. B* **103** 184518
[5] Córdoba R, Baturina T I, Sesé J, Mironov A Yu, Teresa J M De, Ibarra M R, Nasimov D A, KGutakovskii A, Latyshev A V, Guillamón I, Suderow H, Vieira S, Baklanov M R, Palacios J J and Vinokur V M 2013 *Nat. Commun.* **4** 1437
[6] Lin Z, Qin M, Li D, Shen P, Zhang L, Feng Z, Sha P, Miao J, Yuan J, Dong X, Dong C, Qin Q and Jin K 2021 *Supercond. Sci. Technol.* **34** 015001
[7] Lee C S, Jankó B, Derényi I and Barabási A L 1999 *Nature* **400** 337
[8] Ji J, Yuan J, He G, Jin B, Zhu B, Kong X, Jia X, Kang L, Jin K and Wu P 2016 *Appl. Phys. Lett.* **109** 242601
[9] Adami O A, Cerbu D, Cabosart D, Motta M, Cuppens J, Ortiz W A, Moshchalkov V V, Hackens B, Delamare R, Van de Vondel J and Silhanek A V 2013 *Appl. Phys. Lett.* **102** 052603
[10] Koelle D, Kleiner R, Ludwig F, Dantsker E and Clarke J 1999 *Rev. Mod. Phys.* **71** 631
[11] Gol'tsman G N, Okunev O, Chulkova G, Lipatov A, Semenov A, Smirnov K, Voronov B, Dzardanov A, Williams C and Sobolewski R 2001 *Appl. Phys. Lett.* **79** 705
[12] Taylor G G, Morozov D V, Lennon C T, Barry P S, Sheagren C and Hadfield R H 2021 *Appl. Phys. Lett.* **118** 191106
[13] Makhlin Y, Schön G and Shnirman A 2001 *Rev. Mod. Phys.* **73** 357
[14] Clarke J and Wilhelm F K 2008 *Nature* **453** 1031
[15] Bick M, Leslie K E, Binks R A, Tilbrook D L, Lam S K H, Gnanarajan R, Du J and Foley C P 2004 *Appl. Phys. Lett.* **84** 5347
[16] Huang J, Wang H, Wang H, Zhang B, Qian X and Wang H 2019 *IEEE Trans. Appl. Supercond.* **29** 7500604
[17] Han X, Gao M, Wu Y, Mu G, Zhang M, Mei T, Chu P K, Xie X, Hu T and Di Z 2020 *J. Mater. Chem. C* **8** 14605
[18] Makarov D, Volkov O M, Kákay A, Pylypovskyi O V, Budinská B and Dobrovolskiy O V 2022 *Adv. Mater.* **34** 2101758
[19] Wang J, Lin M F, Park S and Lee P S 2018 *Mater. Today* **21** 508
[20] Chortos A, Liu J and Bao Z 2016 *Nat. Mater.* **15** 937
[21] Kenry, Yeo J C and Lim C T 2016 *Microsyst. Nanoeng.* **2** 16043
[22] Mo R, Rooney D, Sun K and Yang H Y 2017 *Nat. Commun.* **8** 13949
[23] Yao B, Zhang J, Kou T, Song Y, Liu T and Li Y 2017 *Adv. Sci.* **4** 1700107
[24] Liang J, Li L, Niu X, Yu Z and Pei Q 2013 *Nat. Photonics* **7** 817
[25] Romaguera A R de C, Doria M M and Peeters F M 2007 *Phys. Rev. B* **75** 184525
[26] Du Q 2005 *J. Math. Phys.* **46** 095109
[27] Xu B, Milošević M V and Peeters F M 2009 *New J. Phys.* **11** 013020
[28] Fomin V M and Dobrovolskiy O V 2022 *Appl. Phys. Lett.* **120** 090501
[29] McKeen L W 2017 *Polyimides, in Film Properties of Plastics and Elastomers* (William Andrew Publishing) Chap. **7** pp. 147–185
[30] Tian W, Chen S, Xu Z, Li D, Du H, Wei Z, Wu K, Sun H, Dong S, Lv Y, Wang Y L, Koelle D, Kleiner R, Wang H and Wu P 2021 *Supercond. Sci. Technol.* **34** 115015
[31] Xu Z, Tian W, Chen S, Yue W, Du H, Li D, Wei Z, Lyu Y Y, Sun H, Wang Y L, Sun G, Chen J, Jin B, Wang H and Wu P 2021 *Supercond. Sci. Technol.* **34** 125012

[32] Pautrat A, Scola J, Goupil C, Simon C, Villard C, Domengès B, Simon Y, Guilpin C and Méchin L 2004 *Phys. Rev. B* **69** 224504
[33] Yanilkin I V, Gumarov A I, Rogov A M, Yusupov R V and Tagirov L R 2021 *Tech. Phys.* **66** 263
[34] Prokhorov V G 1998 *Low. Temp. Phys.* **24** 410
[35] Brandt E H 1993 *Phys. Rev. B* **48** 6699
[36] Brandt E H 1995 *Rep. Prog. Phys.* **58** 1465
[37] Vlasko-Vlasov V K, Colauto F, Buzdin A A, Carmo D, Andrade A M H, Oliveira A A M, Ortiz W A, Rosenmann D and Kwok W K 2016 *Phys. Rev. B* **94** 184502
[38] Zhu C J, Liu L, Song P B, Deng H B, Yi C J, Sun Y K, Wu R, Yin J X, Shi Y, Wang Z and Pan S H 2021 *Chin. Phys. B* **30** 106802
[39] Herrera E, Guillamón I, Galvis J A, Correa A, Fente A, Vieira S, Suderow, Martynovich A Y and Kogan V G 2017 *Phys. Rev. B* **96** 184502
[40] Zhang S S, Yin J X, Dai G, Zheng H, Chang G, Belopolski I, Wang X, Lin H, Wang Z, Jin C and Hasan M Z 2019 *Phys. Rev. B* **99** 161103
[41] Mühlbauer S, Pfleiderer C, Böni P, Laver M, Forgan E M, Fort D, Keiderling U and Behr G 2009 *Phys. Rev. Lett.* **102** 136408
[42] Silhanek A, Guimpel J, Civale L, Lanza H and Levy P 2000 *Physica C* **341** 1217
[43] Silhanek A, Civale L, Candia S, Nieva G, Pasquini G and Lanza H 1999 *Phys. Rev. B* **59** 13620
[44] Paramanik U B, Das D, Prasad R and Hossain Z 2013 *J. Phys.: Condens. Matter.* **25** 265701
[45] Knebel G, Knafo W, Pourret A, Niu Q, Vališka M, Braithwaite D, Lapertot G, Nardone M, Zitouni A, Mishra S, Sheikin I, Seyfarth G, Brison J P, Aoki D and Flouquet J 2019 *J. Phys. Soc. Jpn.* **88** 063707
[46] Womack F N, Adams P W, Valles J M and Cate-lani G 2019 *Phys. Rev. B* **100** 174505
[47] Zhang E, Xu X, Huang C, Zou Y C, Ai L, Liu S, Leng P, Jia Z, Zhang Y, Zhao M, Li Z, Yang Y, Liu J, Haigh S J, Mao Z and Xiu F 2021 *Nano Lett.* **21** 288
[48] Fijałkowski M, Maśka M M, Deniszczyk J and Ślebarski A 2021 *Phys. Rev. B* **104** 165306
[49] Ran S, Liu I L, Eo Y S, Campbell D J, Neves P M, Fuhrman W T, Saha S R, Eckberg C, Kim H, Graf D, Balakirev F, Singleton J, Paglione J and Butch N P 2019 *Nat. Phys.* **15** 1250
[50] Wang Y L, Glatz A, Kimmel G J, Aran-son I S, Thoutam L R, Xiao Z L, Berdiy-orov G R, Peeters F M, Crabtree G W and Kwok W K 2017 *Proc. Natl. Acad. Sci. USA* **114** E10274
[51] Berdiyorov G R, Chao X H, Peeters F M, Wang H B, Moshchalkov V V and Zhu B Y 2012 *Phys. Rev. B* **86** 224504
[52] Saint-James D and Gennes P G 1963 *Phys. Lett.* **7** 306
[53] Barnes L J and Fink H J 1966 *Phys. Rev.* **149** 186
[54] Chen X, Zhan X H, Wang X J, Deng J, Liu X B, Chen X, Guo J G and Chen X L 2021 *Chin. Phys. Lett.* **38** 057402
[55] Cheng Z H, Lei B, Luo X G, Ying J J, Wang Z Y, Wu T and Chen X H 2021 *Chin. Phys. B* **30** 097403
[56] Vijayanand H V, Arunkumar L, Gurubasawaraj P M, Sharma P M V, Basavaraja S, Saleem A, Venkataraman A, Ghanwat A and Maldar N N 2007 *J. Appl. Polym. Sci.* **103** 834